The Productive Conformation of Prostaglandin G 2 at the Peroxidase Site of Prostaglandin Endoperoxide H Synthase: Docking, Molecular Dynamics, and Site-Directed Mutagenesis Studies...

ARTICLE *in* BIOCHEMISTRY · FEBRUARY 2006

Impact Factor: 3.02 · DOI: 10.1021/bi051973k · Source: PubMed

The Productive Conformation of Prostaglandin G_2 at the Peroxidase Site of Prostaglandin Endoperoxide H Synthase: Docking, Molecular Dynamics, and Site-Directed Mutagenesis Studies†

Anthony J. Chubb,‡ Desmond J. Fitzgerald,‡ Kevin B. Nolan,§ and Edelmiro Moman*,§

Centre for Synthesis and Chemical Biology, Department of Pharmaceutical and Medicinal Chemistry, and Department of Clinical Pharmacology, Royal College of Surgeons in Ireland, 123 St. Stephen's Green, Dublin 2, Ireland

Received September 29, 2005; Revised Manuscript Received November 17, 2005

ABSTRACT: We present a plausible productive conformation obtained by docking calculations for the binding of prostaglandin G_2 (PGG_2) to the peroxidase site of prostaglandin endoperoxide H synthase-1 (PGHS-1, COX-1). The enzyme−substrate complex stability was verified by molecular dynamics. Structural analysis reveals the requirements for enzyme−substrate recognition and binding: the PGG_2 15-hydroperoxide group is in the proximity of the heme iron and participates in a hydrogen bond network with the conserved His207 and Gln203 and a water molecule, whereas the carboxylate group forms salt bridges with the remote Lys215 and Lys222. Site-directed mutagenesis showed that a single mutation of Lys215 or Lys222 does not affect enzyme activity, whereas dual mutation of these residues, to either alanine or glutamate, significantly decreases turnover. This indicates that the conserved cationic pocket is involved in enzyme−substrate binding.

Prostaglandin endoperoxide H synthase (PGHS)[1] is a bifunctional membrane enzyme of the endoplasmic reticulum that converts arachidonic acid into prostaglandin H_2 (PGH_2), the precursor of all prostaglandins, thromboxanes, and prostacyclins (*1*−*3*). These lipid mediators are intricately involved in normal physiology, namely, in mitogenesis, fever generation, pain response, lymphocyte chemotaxis, fertility, and contradictory stimuli such as vasoconstriction and vasodilatation, as well as platelet aggregation and quiescence. PGHS is implicated in numerous pathologies, including inflammation (*4*), cancers of the colon (*5*), lung (*6*), and breast (*7*), Alzheimer's disease (*8*), Parkinson's disease (*9*), and numerous cardiovascular diseases (*10*) including atherosclerosis, thrombosis, myocardial infarction, and stroke. Two isoforms of PGHS with different expression patterns (*11*), PGHS-1 and PGHS-2, have been cloned (*12*−*14*) and extensively characterized over the past 2 decades (*15*). The enzyme possesses two spatially and functionally distinct catalytic sites (*16*, *17*). The cyclooxygenase site activity catalyzes the conversion of arachidonic acid to the lipid peroxide prostaglandin G_2 (PGG_2) by stereoselective addition of two oxygen molecules (*18*, *19*) and is the target for nonsteroidal antiinflammatory drugs (NSAIDs) (*20*). The peroxidase site activity catalyzes the two-electron reduction of the hydroperoxide bond of PGG_2 to yield the corresponding alcohol prostaglandin H_2 (PGH_2).

A simplified mechanistic scheme for the cyclooxygenase and peroxidase catalytic cycles is shown in Figure 1 (*21*, *22*). The formation of a phenoxyl radical on Tyr385 couples the activities of the two sites (*23*, *24*). The Tyr385$^\bullet$ radical is produced via oxidation by compound **I**, an oxoferryl porphyrin π-cation radical, which is generated by reaction of the hemin resting state with PGG_2 or other hydroperoxides. The tyrosyl radical homolytically abstracts the 13*proS* hydrogen atom of arachidonic acid which initiates a radical cascade that ends with the stereoselective formation of PGG_2. PGG_2 then migrates (*18*) from the cyclooxygenase (COX) site to the peroxidase (POX) site where it reacts with the hemin group to generate PGH_2 and compound **I**. The heterolytic oxygen−oxygen bond cleavage is assisted by the conserved distal residues His207 and Gln203, mutation of which has been shown to severely impair enzyme activity (*25*). Compound **I**, upon reaction with Tyr385$^\bullet$, gives compound **II**, which in turn is reduced to the hemin resting state by one-electron oxidation of reducing cosubstrates (*26*) or undergoes reactions that result in enzyme self-inactivation (*27*, *28*).

The stereochemical aspects of the cyclooxygenase process are well established (*18*, *29*). X-ray crystallography (*16*, *18*) and site-directed mutagenesis (*19*, *30*), in combination with computational studies, have allowed the identification of the

† This work was supported by the Irish Government under its Programme for Research in Third Level Institutions (K.B.N., E.M.), an Irish Research Council for Science, Engineering and Technology postdoctoral fellowship (A.J.C.), a Health Research Board Programme Grant (D.J.F., K.B.N.), and EU COST D21 (K.B.N.).

* To whom correspondence should be addressed: phone, +353 1 402 2135; fax, +353 1 402 2168; e-mail, emoman@rcsi.ie.

‡ Department of Clinical Pharmacology.

§ Centre for Synthesis and Chemical Biology and Department of Pharmaceutical and Medicinal Chemistry.

[1] Abbreviations: COX, cyclooxygenase; DTT, 1,4-dithio-DL-threitol; EDTA, ethylenediaminetetraacetic acid; GA, genetic algorithm; MS, mass spectrometry; NSAIDs, nonsteroidal antiinflammatory drugs; PGHS, prostaglandin H synthase; POX, peroxidase; PVDF, poly(vinylidene difluoride); RMSD, root mean squared deviation; ROS, reactive oxygen species; SD, standard deviation; SDS−PAGE, sodium dodecyl sulfate−polyacrylamide gel electrophoresis; TAE, Tris−acetate−EDTA.

10.1021/bi051973k CCC: $33.50
Published on Web 00/00/0000 PAGE EST: 9.5

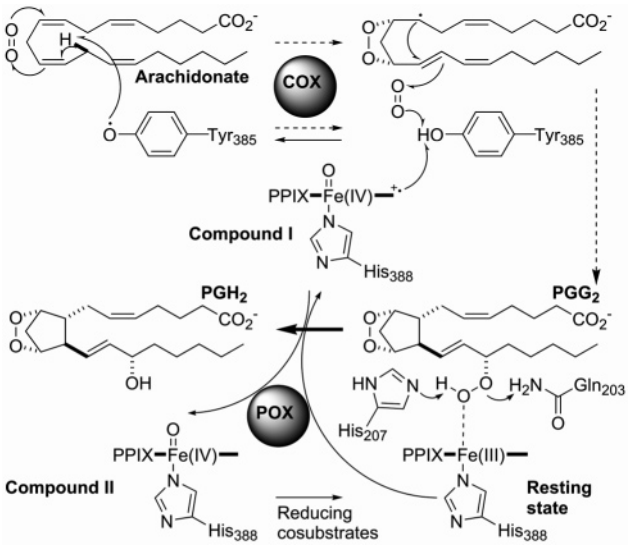

FIGURE 1: Cyclooxygenase and peroxidase catalytic cycles of PGHS.

enzyme residues involved in substrate binding and positioning (*18*) as well as the elucidation of the productive conformation of arachidonic acid (*31*), other substrates, metabolites, and inhibitors. This structural knowledge has been applied to the rational design of potent inhibitors of the cyclooxygenase activity, including numerous with isoform selectivity (*20*). The cyclooxygenase pocket is deeply buried within the protein at the end of an essentially hydrophobic channel, the entrance of which is at the membrane binding domain and continues to Tyr385, adjacent to the heme group (*16*). In contrast, the peroxidase pocket is a broad cavity on the surface of the protein. This allows small molecules to rapidly diffuse in and out of this pocket, which, together with the hemin reactivity, explains the lack of reported crystal structures of substrates or products bound to the iron. Peroxidase catalysis can continue independently of the cyclooxygenase site activity (*28*) (see Figure 1) and is a source of free radicals and reactive oxygen species (ROS), which may contribute to tissue damage or thrombosis (*32*). However, it is impossible to genetically eradicate both isoforms of PGHS in a living organism (*33*), and thus a pharmacological approach is necessary to elucidate the role of this peroxidase in pathophysiology. To facilitate the rational design of potent and selective inhibitors of this site (*34*, *35*), we decided to elucidate the catalytically active conformation of PGG_2 in PGHS−POX.

To gather relevant information on the structural features necessary for enzyme−substrate recognition and binding at the peroxidase site, we combined docking and molecular dynamics (MD) in silico studies with site-directed mutagenesis experiments. The recent publication of a theoretical docking−MD study (*36*) using a nonnatural PGG_2 analogue and a different docking methodology has prompted us to report our results with the natural substrate. Our computational and mutagenesis studies, correlated with previous knowledge in the field, provide a plausible binding model of PGG_2 within the peroxidase site of PGHS-1.

EXPERIMENTAL PROCEDURES

Reagents. Unless otherwise stated, all reagents were obtained from Sigma-Aldrich.

Docking Studies. Ligands were constructed using the SYBYL software package version 6.91 (Tripos Inc.) and geometry-optimized with MOPAC at the PM3 level of theory. A 2.0 Å resolution crystal structure of ovine PGHS-1 (*37*) (PDB code 1Q4G) was used for the docking and molecular dynamics experiments. All molecules except chain A and heme A were removed. Hydrogens were then added and minimized. The carbon atoms of the protoporphyrin ring were defined as aromatic, C.ar in the Tripos Force Field notation, and the four nitrogen atoms as N.pl3, to obtain a smooth homogeneous distribution of charges. Kollman all-atom charges were assigned to the protein, and Gasteiger−Hückel charges were computed for the protoporphyrin group. A 1.0 formal charge was assigned to the iron atom (similar docking results were obtained with a charge of 1.6; values of 2.0 and 3.0 resulted in overestimation of the electrostatic term of the docking energies). Docking experiments were carried out using the Lamarckian genetic algorithm implemented in the automated docking program Autodock, version 3.0.5 (*38*). The ligand and the protein were prepared for docking with Autodock Tools. Autogrid was used to generate the grid maps for an approximately $23 \times 23 \times 23$ Å^3 cell box centered above the heme iron. Autodock stochastically generates a population of conformational, rotational, and translational isomers from any given starting structure of the ligand and docks them within the active site of the protein, represented by a series of fixed-coordinate grid maps. Each ligand conformation is represented by a chromosome constituted by genes representing ligand conformational, rotational, and translational degrees of freedom. The individuals are evaluated by a fitness function which assesses the total interaction energy between the protein and the ligand molecule, the internal energy of the ligand, and the desolvation/solvation energies for the formation of the protein/ligand complex (the sum of these three terms is referred to as "docking energy" in this paper). Individuals in the population are selected for reproduction in accordance with their fitness and undergo mutation and crossover reproduction operators to generate new individuals. A number of generations are permitted (see below), and the fittest individual is chosen. The whole evolutionary process was repeated 256 times (genetic algorithm runs), which resulted in a database of 256 individuals. To ensure that the results were independent from the starting conformation of the ligand, a stochastic conformational database of PGG_2 was created using the Tripos force field, and the docking calculations were repeated 10 times using the minimum energy conformer and another 10 times using 10 different conformers randomly chosen from the database as starting structures for Autodock. Default parameters were employed except for the following: number of GA runs, 256; maximum number of energy evaluations, 2.5×10^6; maximum number of generations, 2.7×10^5; internal electrostatic energy computed. A more in-depth experiment was performed with 2.5×10^7 energy evaluations and 2.7×10^6 generations. The distances and energies reported here are those obtained in this later experiment unless otherwise stated. The two possible protonation states for distal histidine 207 were also considered, and the docking results obtained were similar in all cases.

Homology Modeling. Ovine PGHS numbering is used. A homology modeling structure of human PGHS-1 was constructed using the Swiss-Model server (*39*) and the ovine

crystal structure 1Q4G as template. After preparation of the human protein in SYBYL, the heme group was merged into the POX site, and the complex was hydrated with ~16000 explicit water molecules using the Molecular Silverware algorithm in an approximately 90 × 90 × 90 $Å^3$ cell box. The system was minimized using the Tripos force field, allowing 1000 iterations, and the solvent was removed. The results of the docking experiments with the modeled human enzyme were identical to those with the ovine crystal structure. PGHS homologues from all mammalian species for which a homologue exists were aligned using the ClustalW (*45*) program (Figure 5). Protein sequences were obtained from the National Centre for Biotechnology Information (NCBI) GenBank database and are listed in the Supporting Information.

Molecular Dynamics. The PGG_2 conformer with the most favorable docking energy was merged into the PGHS-1 ovine structure. The complex was hydrated as described above and then minimized in two steps: first, the water molecules were minimized using 1000 iterations with the coordinates of the protein fixed, and, second, the whole system was minimized using 1000 iterations. A 500 ps molecular dynamics experiment was carried out in SYBYL using the Tripos force field and the NTV ensemble (constant number of particles, temperature, and volume) at 300 K with periodic boundary conditions. Default parameters were used and snapshots recorded every 0.5 ps.

Site-Directed Mutagenesis. Site-directed mutations in human PGHS-1 were prepared using the QuikChange site-directed mutagenesis kit supplied by Stratagene (La Jolla, CA) as described previously (*46*). Initially, a hexahistidine tag was inserted between the signal peptide and mature peptide chain of human PGHS-1 (*12*) in the mammalian expression vector pcDNA3-hCOX-1, using primers described elsewhere (*43*). This template (pcDNA3-H_6COX-1) was then sequentially mutated using the following primers (5′ to 3′): K211A, ACCCACCAGTTCTTCGCAACTTCTGGCAAGATG; K215A, TTCAAAACTTCTGGCGCGATGGGTCCTGGCTTC; K222A, GGTCCTGGCTTCACCGCGGCCTTGGGCCATGGG; K211E, ACCCACCAGTTCTTCGAAACTTCTGGCAAGATG; K215E, TTCAAAACTTCTGGCGAGATGGGTCCTGGCTTC; K222E, GGTCCTGGCTTCACCGAGGCCTTGGGCCATGGG; and the reverse/complementary sequences thereof. Each mutation was verified by DNA sequencing, using either forward, GGGAACCAAAGGGAAGAAGC, or reverse primers AAAGCTGCTCATCGCCCCAG (5′ to 3′). All DNA sequencing was done commercially (AGOWA, Germany), the results of which appear in the Supporting Information, Figure S1. Single mutants were used as templates for the subsequent successive construction of double and triple mutants. Transfection grade DNA was isolated from transformed *Escherichia coli* using an alkaline lysis and anion-exchange method, as per the manufacturer's instructions (Qiagen). Plasmid size was verified by separation in a 0.8% (w/v) agarose TAE gel, after digestion with *Bam*HI and *Xho*I and intercalation by ethidium bromide (data not shown).

Transient Expression of Human PGHS-1 Mutants. Wild-type and mutant pcDNA3-hCOX-1 constructs were transiently expressed in COS-1 cells as described previously (*46*). Parental vector pcDNA3 was used as a control for all transfection experiments. COS-1 cells (400000 per well) were grown in 2 mL of Dulbecco's modified Eagle's medium, 10% fetal bovine serum, 100 units of penicillin, and 100 μg/mL streptomycin in six-well plates at 37 °C and 5% CO_2. Purified plasmid DNA (2.0 μg) was transfected into COS-1 cells using 10 μL of LipofectAMINE (Invitrogen) for 24 h, in duplicate, as described in the manufacturer's protocol. The DNA/LipofectAMINE mixture was allowed to settle for 5 h prior to 1:2 dilution with 20% fetal bovine serum.

Assay of Prostaglandins Synthesized by Transfected COS-1 Cells. Forty-eight hours after transfection the cells were assayed for PGHS-1 activity by stimulation with 60 μM arachidonic acid for 15 min in HEPES-buffered Hank's saline solution. The PGE_2 product was assayed using an enzyme-linked immunoassay for PGE_2 (Assay Designs, Ann Arbor, MI). Assays were performed using 100 μL of 1:50 diluted samples, as per the manufacturer's instructions. The cells were harvested with 1 mL of 1% $C_{10}E_6$ (Albion), 100 mM NaCl, 25 mM Na_2HPO_4 (pH 7.8), 20 mM imidazole, and 1× EDTA-free protease inhibitors (Calbiochem).

Western Blotting. Standard Western blotting was performed, as described previously (*47*). Equal volumes (24 μL) of each cell lysate sample were separated in a reducing 10% acrylamide SDS−PAGE gel, transferred to PVDF membranes, and probed using an anti-human PGHS-1 monoclonal antibody (Cayman Chemicals) and a horseradish peroxidase-linked anti-mouse IgG secondary antibody (Amersham). West-pico chemiluminescence reagents (Pierce) were used to illuminate the PGHS-1 protein, the autoradiography of which is shown.

Molecular Graphics. Molecular graphics images were produced using the UCSF Chimera package (*48*) from the Computer Graphics Laboratory, University of California, San Francisco. UCSF Chimera computes solvent-excluded molecular surfaces using MSMS (*49*).

RESULTS

Docking Studies. The first X-ray structure of ovine PGHS-1 (oPGHS-1) cocrystallized with a ligand, a serendipitous glycerol molecule, in the peroxidase site has recently been reported (*37*) (PDB code 1Q4G). This 2.0 Å resolution structure was used for the docking and dynamics experiments reported here. The structure of natural PGG_2 was docked into the peroxidase pocket of the protein using the Lamarckian genetic algorithm implemented in the automated docking program Autodock (*38*) (see Experimental Procedures). For analysis of the results, docked ligand conformers within 0.5 Å root mean squared deviation (RMSD) were assumed to be identical and grouped into the same cluster, and the docking energy of the best fit individual was assigned to each cluster. The clusters were arranged in ascending (less negative) docking energies, and only those within 6.0 kcal/mol from the minimum were considered in the analysis. Similar clustering distributions were consistently observed in all of the experiments. A refined experiment with a 10-fold increase in the number of generations was also performed, providing a similar cluster distribution but improved by ~1.0 kcal/mol. The docking energies obtained were −15.7 kcal/mol for the in-depth experiment and −15.3 kcal/mol for the best standard experiment.

A conserved binding mode was identified. The structure of the conformer of PGG_2 with the most favorable docking

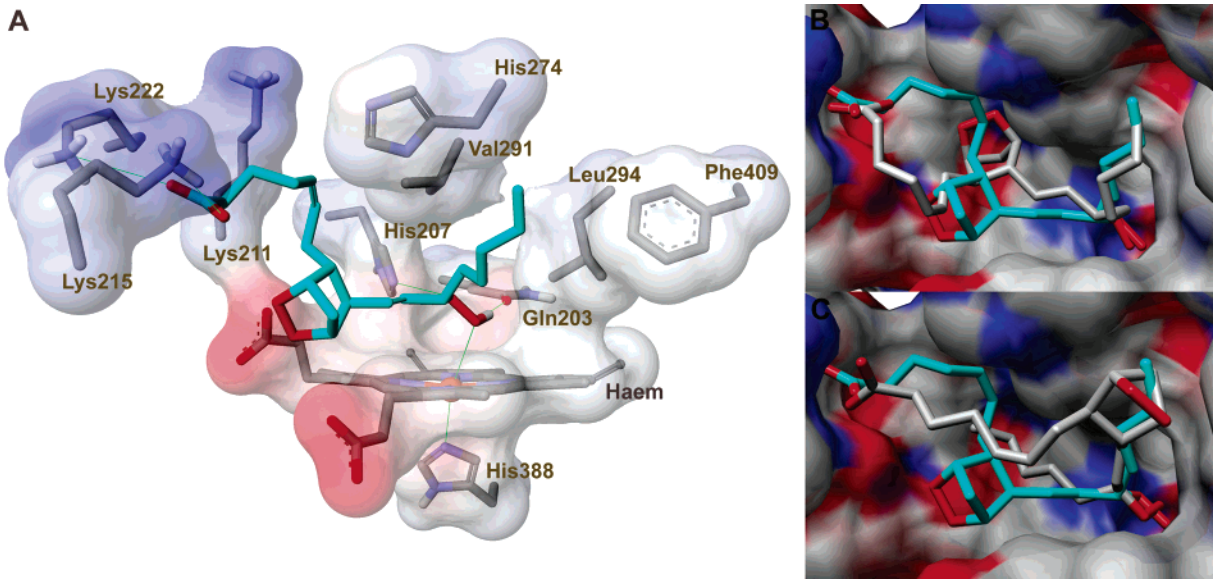

FIGURE 2: Model of PGG_2 bound to the PGHS-1 peroxidase site. (A) Model of the catalytically competent conformation of PGG_2 bound to the PGHS-1 peroxidase site. (B, C) Minimum docking energy PGG_2 conformer (carbons in blue) superimposed on other possible productive conformations (carbons in gray) within the PGHS−POX active site, represented by molecular surfaces.

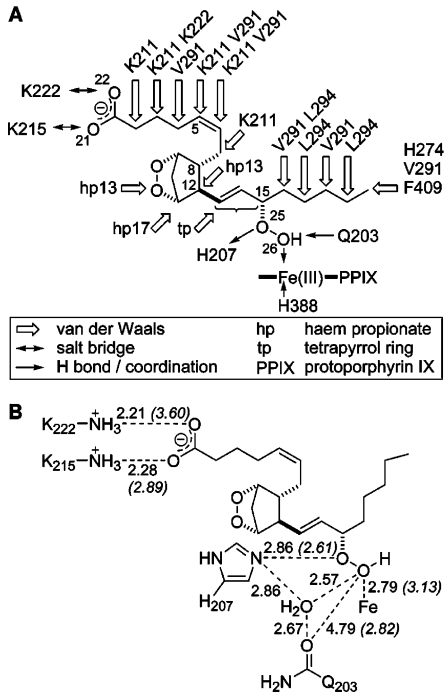

FIGURE 3: PGG_2−PGHS-1 peroxidase interactions. (A) Schematic dissection of the most important PGG_2−PGHS−POX interactions. (B) Salt bridges and hydrogen bond networks. Distances (Å) before (italics in parentheses) and after minimization.

energy, consistently obtained from all the docking experiments, and the active site residues that interact most directly with the substrate are shown in Figure 2A. Solvent-accessible surfaces are displayed to enhance the three-dimensional perception of the peroxidase pocket. More detailed information on the enzyme−substrate interactions is shown in Figure 3.

A model of human PGHS-1 (hPGHS-1) was constructed using the Swiss-Model server (*39*) and oPGHS-1 as a template as there is 91% overall sequence identity between the ovine and the human enzymes and the POX site residues are entirely conserved. The standard docking experiment was repeated three times with the human model providing essentially identical results to those obtained with the ovine structure.

The terminal oxygen of the 15-hydroperoxide group (O26) is ~3.0 Å from the heme iron, the same distance as the oxygen atom of the glycerol molecule present in the crystal structure, and at a hydrogen bond distance from the carbonyl oxygen of the Gln203 side chain. The inner oxygen of the hydroperoxide (O25) is located at a hydrogen bond distance from the nitrogen of His207. These two residues have previously been mutated and are known to be essential for the catalytic activity of the enzyme (*25*). On the other hand, one of the oxygen atoms of the carboxylate group (O22) of PGG_2 is in the proximity of the positively charged nitrogen of Lys222, while the other (O21) is in the proximity of Lys215 and the backbone nitrogen of Gly214 (not shown for clarity). The implication of these remote lysine residues in substrate binding has not previously been addressed.

The 9,11-endoperoxycyclopentane moiety of PGG_2 is inserted between the two propionate side chains of the heme (Figure 3A), while the C13−C15 fragment of PGG_2 lies parallel to the tetrapyrrole plane (Figure 2A). The side chain comprising carbons C2−C7 of PGG_2 is inserted between Val291 and, more importantly, the lipophilic segment of Lys211. The C16−C20 side chain is positioned in the hydrophobic pocket defined by residues Val291, Leu294, and Phe409 and the methylene carbon of His274.

Two additional catalytically competent conformations of PGG_2, with higher docking energies, were identified. Panels B and C of Figure 2 represent the two conformers (carbons in gray) superimposed with the structure of the minimum docking energy conformer (carbons in blue) within the active site of the enzyme (molecular surfaces). Catalytically competent or "productive" conformations were defined as those in which the terminal hydroperoxide oxygen atom of PGG_2 (O26) is located within 4.0 Å of the iron. The computed docking energies for conformers in (B) and (C) are −13.3 and −13.7 kcal/mol, respectively (Figure 2).

The high degree of complementarity between the three conformers and the peroxidase pocket is noteworthy (Figure

2). Indeed, all fulfill four structural requirements: (i) the hydroperoxide group is in the vicinity of the heme iron, His207, and Gln203, an established prerequisite for catalytic activity (*25*); (ii) the carboxylate group is near the cationic pocket comprising Lys215 and Lys222; (iii) a lipophilic moiety points toward the Val291, Leu294, His273, and Phe409 hydrophobic pocket; and (iv) another lipophilic moiety is inserted between Val291 and Lys211. Furthermore, the distance between the two polar anchor points, the iron on one side and Lys215 and Lys222 on the other, forces the substrate to adopt an extended conformation, approximately 14 Å between the terminal hydroperoxide oxygen (O26) and the more distant carboxylate oxygen (O22). This limits the possible productive conformations of PGG_2 to the three reported here (Figure 2).

It is noteworthy that the docking model reported by Seibold et al. (*36*) for a PGG_2 analogue in some way resembles one of the conserved binding modes found by us for the natural substrate (Figure 2C), except for the fact that the carboxylate group of the PGG_2 analogue points outward from the pocket and is solvated by water molecules, whereas in our model the carboxylate group of the native substrate interacts with Lys215 and Lys222 in all cases.

Molecular Dynamics. To account for protein flexibility and the possible participation of water molecules in substrate binding, the most favorable complex structure (Figure 2A) was hydrated with ~16000 explicit water molecules and energy minimized, and a 500 ps molecular dynamics simulation was performed at 300 K using the Tripos force field, the NTV ensemble, and periodic boundary conditions. Although native PGHS is a membrane-bound homodimeric protein inserted into one leaflet of the lipid bilayer, we think that the dynamics conditions employed are adequate because (1) the detergent needed to extract the enzyme is not necessary for enzyme assays (*25*), indicating stable enzyme activity in detergent-free water; (2) a 2 ns molecular dynamics simulation carried out previously (*36*) showed that the enzyme is stable as a monomer in aqueous media; (3) the peroxidase site is located distal to the membrane binding domain and the dimerization domain; and (4) the crystal structure of the monomeric (*31*) enzyme does not significantly differ from those of the dimeric and multimeric crystal structures.

Particularly significant protein−ligand distances are shown in Figure 3B both before (in parentheses) and after minimization. Slight conformational modifications that optimize substrate binding take place in the complex upon minimization. The distances between the positively charged nitrogen atoms of Lys215 and Lys222 and the negatively charged oxygen atoms of the substrate carboxylate are shortened. The Fe−O26 distance also shortens, mainly due to the realignment of the heme iron into the protoporphyrin plane. This is likely to be a computational artifact due to the lack of adequate bending parameters for a pentacoordinated heme iron in the Tripos force field (Sybyl version 6.9). However, this approximation should not appreciably affect the accuracy of the simulation for the purposes of this work.

Interestingly, the hydrogen bond network between PGG_2 15-hydroperoxide, His207, and Gln203 is modified upon minimization to incorporate a water molecule, almost equidistant between PGG_2−O26, His207, and Gln203. Gln203 retreats backward to allow the insertion of the water

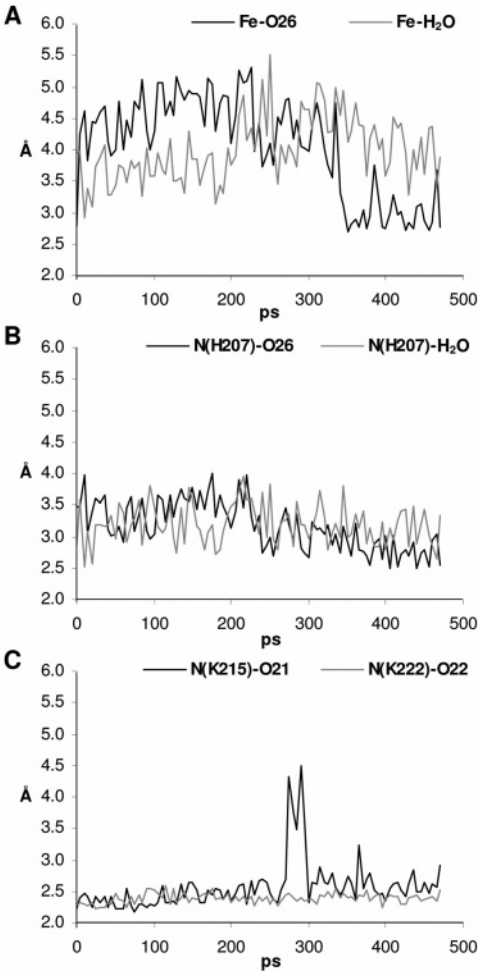

FIGURE 4: Molecular dynamics of PGG_2 bound to the PGHS−POX site. Most relevant enzyme−substrate distances (Å) along the 500 ps molecular dynamics simulation.

and interacts with the substrate only indirectly through this water molecule. This hydrogen bond network incorporating the water molecule is maintained along the dynamics experiment and is therefore unlikely to be a computational artifact (Figure 4). In fact, it has been hypothesized (*40*) that the ability to immobilize a water molecule in the vicinity of the catalytic center might be an intrinsic structural feature of peroxidases, responsible in part for the different catalytic mechanisms of peroxidases (one-electron oxidants) and catalases (two-electron oxidants).

The overall folding of the protein is maintained along the dynamics experiment, and the enzyme−substrate complex is stable, with a C_α RMSD of 1.33 Å for the last 90% of the dynamics simulation. The evolution of various relevant enzyme−substrate distances along the 500 ps dynamics simulation is shown in Figure 4. Interestingly, a water molecule and the terminal hydroperoxide oxygen (O26) alternately occupy a position close to the iron (Figure 4A). We hypothesize that before ligand binding this water molecule, immobilized by the hydrogen bond network with highly conserved His207 and Gln203 (Figure 5) and weakly coordinated to the heme iron, might occupy the same position at the distal side of the peroxidase pocket as the glycerol oxygen atom bound to iron in the 1Q4G crystal structure (*37*). The water molecule would be displaced by the hydroperoxide group of the substrate and, instead of diffusing

		Q203 H207 K211 K215 K222	
Guinea pig	**PGHS-2**	FFA*Q*HFT*H*QFF**K**SDQ**K**RGPAFTTGLA	211
Boar	**PGHS-2**	FFA*Q*HFT*H*QFF**K**SDQ**K**RGPAFTTGLA	211
Mouse	**PGHS-2**	FFA*Q*HFT*H*QFF**K**TDH**K**RGPGFT**R**GLG	211
Brown rat	**PGHS-2**	FFA*Q*HFT*H*QFF**K**TDQ**K**RGPGFT**R**GLG	211
Cotton rat	**PGHS-2**	FFA*Q*HFT*H*QFF**K**TDQ**K**RGPGFT**R**GLG	211
Gerbil	**PGHS-2**	FFA*Q*HFT*H*QFF**K**TDQ**K**RGPGFT**R**GLG	211
Rabbit	**PGHS-2**	FFA*Q*HFT*H*QFF**K**TDL**K**RGPAFT**K**GLG	211
Dog	**PGHS-2**	FFA*Q*HFT*H*QFF**K**TDH**K**RGPAFT**K**GLG	211
Mink	**PGHS-2**	FFA*Q*HFT*H*QFF**K**TDH**K**RGPGFT**K**GLG	211
Horse	**PGHS-2**	FFA*Q*HFT*H*QFF**K**TDP**K**RGPAFT**K**GLG	211
Hamster	**PGHS-2**	FFA*Q*HFT*H*QFF**K**TDQ**K**RGPGFT**R**GLG	82
Chimp	**PGHS-2**	FFA*Q*HFT*H*QFF**K**TDH**K**RGPAFTNGLG	347
Human	**PGHS-2**	FFA*Q*HFT*H*QFF**K**TDH**K**RGPAFTNGLG	211
Sheep	**PGHS-2**	FFA*Q*HFT*H*QFF**K**TDIERGPAFT**K**GKN	210
Cow	**PGHS-2**	FFA*Q*HFT*H*QFF**K**TDFERGPAFT**K**GKN	206
Human	**PGHS-1**	FFA*Q*HFT*H*QFF**K**TSG**K**MGPGFT**K**ALG	224
Chimp	**PGHS-1**	FFA*Q*HFT*H*QFF**K**TSG**K**MGPGFT**K**ALG	408
Sheep	**PGHS-1**	FFA*Q*HFT*H*QFF**K**TSG**K**MGPGFT**K**ALG	225
Boar	**PGHS-1**	FFA*Q*HFT*H*QFF**K**TSG**K**MGPGFT**K**ALG	126
Dog	**PGHS-1**	FFA*Q*HFT*H*QFF**K**TSG**K**MGPGFT**K**ALG	258
Rabbit	**PGHS-1**	FFA*Q*HFT*H*QFF**K**TSG**K**MGPGFT**K**ALG	231
Mouse	**PGHS-1**	FFA*Q*HFT*H*QFF**K**TSG**K**MGPGFT**K**ALG	227
Gerbil	**PGHS-1**	----------TSG**K**MGPGFT**K**ALG	5
Brown rat	**PGHS-1**	FFA*Q*HFT*H*QFF**K**TSG**K**MGPGFT**K**ALG	227
Cow	**PGHS-1**	FFA*Q*HFT*H*QFF**K**TSG**K**MGPGFT**K**ALG	105
consensus		***********:. : **.** .	

FIGURE 5: Evolutionary conservation of the cation pocket. All available mammalian PGHS sequences were aligned using ClustalW (*45*). See Supporting Information for full species name and GenBank accession numbers. The consensus line indicates identity in all sequences (*) or the occurrence of either conserved (:) or semiconserved (.) substitutions. Catalytic residues Glu203 and His207 are in italics, Lys211, Lys215, and Lys222 and positive substitutions thereof are in bold, and human PGHS-1 and -2 are underlined. Original open reading frame numbering is shown.

away from the pocket, would be pushed toward Gln203, forcing this residue to retreat backward, initiating a rearrangement of the hydrogen bond network (Figure 3B). This is corroborated by the finding that both the O26 of PGG_2 and the water molecule tend to stay at a hydrogen bond distance from His207 during the dynamics simulation (Figure 4B).

Significantly, the salt bridges between Lys215 and Lys222 and the PGG_2 carboxylate group are tightly conserved throughout the dynamics experiment (Figure 4C), suggesting that this interaction plays a critical role in enzyme−substrate binding.

Site-Directed Mutagenesis. The presence of positively charged residues in the environment of the active site of a protein facilitates the binding of negatively charged substrates (*41*, *42*). Indeed, Arg120 has been demonstrated to play a crucial role in substrate binding at the cyclooxygenase site of PGHS-1, and the mouth of the hydrophobic channel that directs substrates to the cyclooxygenase site is rich in positively charged residues, namely, Arg79 and Arg83. However, to the best of our knowledge, the roles of Lys215 and Lys222 at the PGHS peroxidase site in PGG_2 binding have not previously been demonstrated. In accordance with our model, the loss of the salt bridges between the PGG_2 carboxylate group and these two lysines, due to mutation, should result in a significant decrease of enzyme−substrate affinity and thus reduced enzyme efficiency.

Lys211 is also located near Lys215 and Lys222 (Figure 2A). Despite the fact that our modeling studies do not suggest participation of Lys211 in establishing a polar interaction

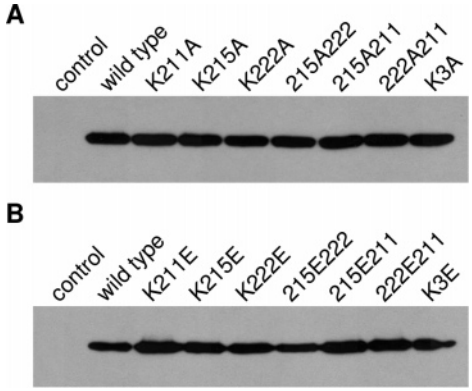

FIGURE 6: Western blot analysis of PGHS-1 mutants. Cell lysates of COS-1 cells transiently expressing mutant forms of His-tagged PGHS-1 were subjected to Western blotting and probed using an anti-PGHS-1 monoclonal antibody. Wild-type human PGHS-1 and control cells transfected with the parental vector are shown for comparison. (A) Lys-Ala. (B) Lys-Glu. Mutant abbreviations are as follows: 215A222, K215A/K222A; 215A211, K211A/K215A; 222A211, K211A/K222A; K3A, K211A/K215A/K222A; 215E222, K215E/K222E; 215E211, K211E/K215E; 222E211, K211E/K222E; K3E, K211E/K215E/K222E.

with PGG_2 carboxylate, it is geometrically conceivable that a catalytically competent conformation of the substrate may form an ionic linkage with this residue. We therefore included Lys211 in our mutagenesis studies.

Site-directed mutagenesis of human PGHS-1 was performed sequentially, producing all combinations of single, double, and triple mutations. Thus, 14 mutants of the enzyme were constructed: 3 single mutants with a lysine to alanine replacement (K215A, K222A, and K211A), 3 single mutants with a lysine to glutamic acid replacement (K215E, K222E, and K211E), 3 double mutants with lysine to alanine replacements (K215A/K222A, K211A/K215A, and K211A/K222A), 3 double mutants with lysine to glutamic acid replacements (K215E/K222E, K211E/K215E, and K211E/K222E), 1 triple mutant with the three lysines replaced by alanine (K211A/K215A/K222E), and 1 triple mutant with the three lysines replaced by glutamic acid (K211E/K215E/K222E). The mutants were produced in the mammalian expression vector pcDNA3 containing recombinant human histidine-tagged PGHS-1 (*12*, *43*). COS-1 cells were transiently transfected with the human PGHS-1 mutants, and equal volumes of cell lysate fractions were analyzed by Western blotting (Figure 6). These data indicate that all mutants were similarly overexpressed by the human cytomegalovirus immediate−early enhancer−promoter in the pcDNA3 mammalian expression vector and translated into proteins showing the same relative molecular weight as the wild-type enzyme (Figure 6).

To test the enzymatic activity of the PGHS-1 mutants, the transiently transfected COS-1 cells were allowed to react with arachidonic acid substrate for 15 min before the media were removed and assayed for PGE_2 accumulation using an enzyme-linked immunosorbent assay. COS-1 cells transfected with parental pcDNA3 vector DNA showed no activity. Furthermore, preincubation of wild-type transfected cells with aspirin, which covalently inactivates the COX site of PGHS at Ser530 (*44*), shows baseline activity, verifying that PGE_2 accumulation seen in this assay is PGHS dependent. The assays were performed in duplicate wells, with PGE_2 accumulation in each well assayed in duplicate, on three

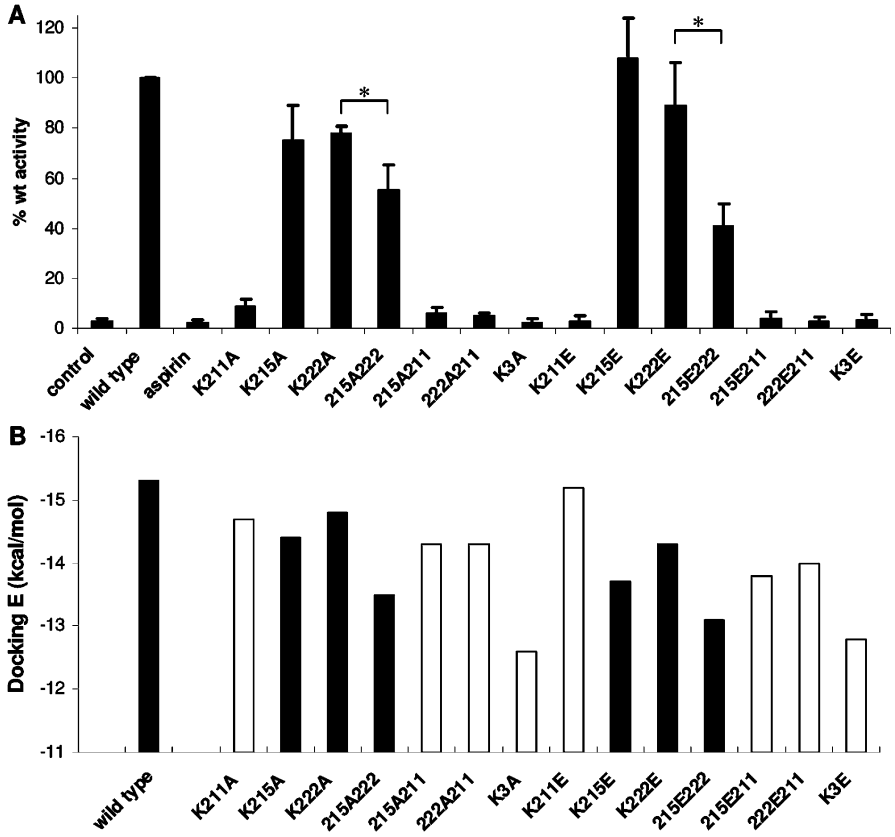

FIGURE 7: Activity of PGHS-1 mutants in transiently transfected mammalian cells. (A) Transiently transfected COS-1 cells were assayed for PGE_2 production following arachidonic acid stimulation. PGE_2 produced was converted to a percentage of wild-type activity ($n = 3$, SD). A preincubation with acetylsalicylic acid (aspirin) was used to show COX dependence in this assay. The asterisk indicates $P < 0.05$. Mutant abbreviations are as in Figure 6. (B) Docking energies (kcal/mol) for the best productive conformation of PGG_2 bound to the peroxidase site of each of the reported mutants.

separate occasions, thus accounting for possible slight variations in PGHS-1 or PGE_2 synthase expression levels. The amount of PGE_2 produced by each of the mutants was converted to a percentage of that produced by the wild-type enzyme (Figure 7A). The most striking effect is the complete abolition of activity in all mutations involving Lys211. It is also clear that single mutations involving Lys215 and Lys222, to either alanine or glutamic acid, do not impair PGHS activity, with these mutants showing essentially wild-type conversion of PGG_2 to PGH_2, which is in turn converted by synthases to the PGE_2 measured in our experiments. Importantly, when both of these residues are simultaneously mutated, a significant reduction of 27% and 58% was noted for alanine or glutamate, respectively. This reduction is statistically relevant, with variance between the Lys222 and Lys215/Lys222 double mutants showing paired Student's *t*-test *P* values of 0.038 and 0.021 for the alanine and glutamate mutants, respectively.

DISCUSSION

Our docking and molecular dynamics studies have shown that there are two polar anchor points for PGG_2 within the PGHS-1 peroxidase pocket. First, in agreement with the commonly accepted mechanism, the location of the 15-hydroperoxide group within the iron coordination sphere is a requirement for catalysis. Second, the carboxylate group of PGG_2 establishes salt bridges with Lys215 and Lys222. Furthermore, the concomitant binding of PGG_2 hydroperoxide in the vicinity of the iron and the carboxylate close to the lysines requires the substrate to adopt an extended geometry that narrows the set of possible productive conformers to the ones reported here, with minor variations.

The results in Figure 7A show the importance of Lys211, Lys215, and Lys222. Mutation of Lys211 completely impairs the activity of the enzyme. This effect is too dramatic to be attributed to a perturbation of ligand binding and is more consistent with a severe alteration of the structure of the enzyme. Indeed, this residue is totally conserved across both PGHS isoforms sequenced from species spanning a broad taxonomic range (Figure 5) and structurally is found near the end of helix H2 (*16*), which also contains the catalytic Glu203 and His207 residues. Figure 8 shows how, through formation of ionic linkages with the similarly conserved residues Asp236 and Glu290, Lys211 acts as a bridge between three poorly organized regions of the protein in the vicinity of the peroxidase pocket (*16*). In addition, the N−O distances between the ammonium group of Lys211 and the carboxylate groups of Asp236 and Glu290 are completely conserved along the molecular dynamics simulation (Figure 9A,B), whereas the N−O distance between the ammonium group Lys211 and the carboxylate group of PGG_2 is never less than 8 Å (data not shown).

The binding energies obtained after docking PGG_2 into the peroxidase catalytic pocket of each of the reported mutants are shown in Figure 7B. In all cases the lowest energy catalytically competent conformer is similar to that observed for the wild-type protein (note that the carboxylate group of PGG_2 is still able to form a hydrogen bond with

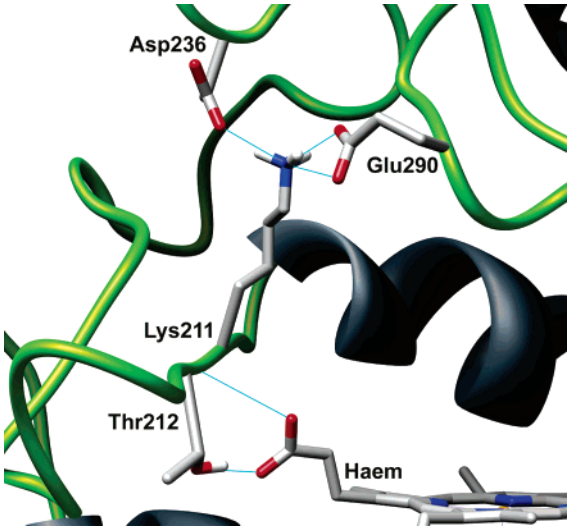

FIGURE 8: Structural role of Lys211. The backbone of PGHS-1 is shown in ribbon diagram, while the heme and side chains of Lys211, Asp236, Glu290, and Thr212 are depicted as sticks.

the backbone NH of Gly214). However, in a few cases, the lowest energy catalytically competent conformer is not the absolute lowest energy conformer. In no case was the PGG_2 carboxylate found close to the Lys211 ammonium. It is noteworthy that the trend in predicted docking energies for the single and double mutants involving Lys215 and Lys222 (Figure 7B, solid bars) is similar to that found in the biological activity assays. For 215A222 and 215E222, in which the two salt bridges are lost, the decrease in docking energies is approximately 2.0 and 2.5 kcal/mol, respectively, which translates into a 30−60% decrease of enzymatic activity. In all cases, including all of the Lys211 mutants for which the enzymatic activity is completely impaired (Figure 7B, empty bars), the substrate can still access the active site and the binding energies are comparable. For instance, the affinity of the substrate toward K211E should, according to our docking data, be as good as that for the wild-type enzyme. However, like all other mutants involving Lys211, it is completely inactive. These results indicate that (i) in terms of substrate affinity, any of the mutations should have either a moderate (as empirically demonstrated for 215A222 and 215E222) or negligible (as empirically demonstrated for K215A, K222A, K215E, and K222E) effect on enzyme activity; and (ii) a complete abolition of the enzymatic activity (as observed in all of the K211 mutants) is, in this particular case, unlikely to be the result of a mere perturbation on substrate binding.

Importantly, the Phe209−Leu230 segment, which contains Lys211 and connects helix H2 to H3, includes Thr212, which forms hydrogen bonds with the C13 heme propionate (Figures 8 and 9C) and is likely to be crucial for heme binding (*37*). Lysine 211 is, therefore, likely to have a structural function, and its replacement could prevent the correct folding of the peroxidase site and thus its ability to recruit the heme group. Furthermore, we consider that the conformational change required for Lys211 to participate in ligand binding is unlikely to be compatible with its apparent structural role. Final proof of the involvement of Lys211 in cross-linking and stabilization of the large loop comprising the distal "roof" of the peroxidase site awaits further characterization and testing. It would be informative to

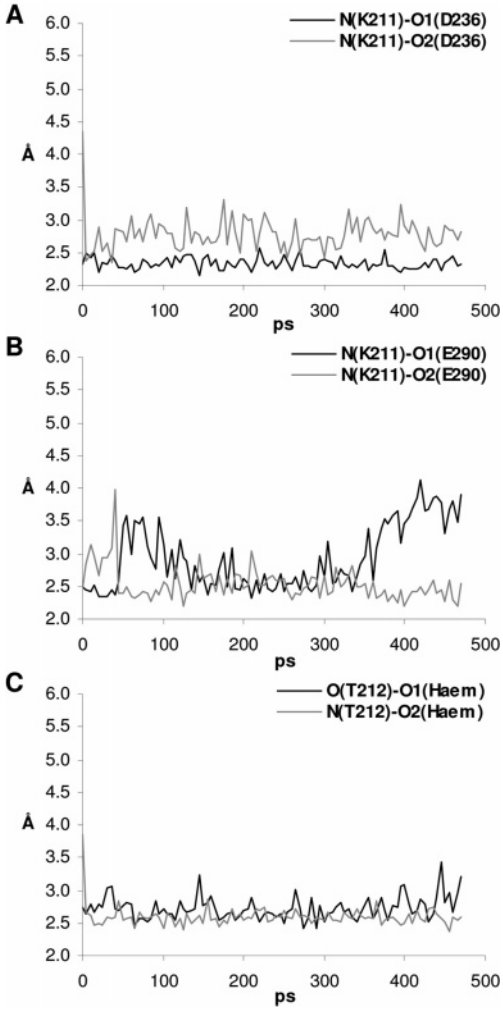

FIGURE 9: Molecular dynamics showing conservation of salt bridges. The preservation of the salt bridges between the ammonium nitrogen of Lys211 and the carboxylate oxygens of Asp236 (A) and Glu290 (B) during the molecular dynamics simulation is illustrated by monitoring interatomic bond lengths (Å). The maintenance of a hydrogen bond between the hydroxyl group and the backbone amide of Thr212 and the C13 heme propionate was also monitored (C).

attempt to restore enzyme activity by mutating the residues involved in salt-bridging interactions with Lys211, namely, Asp236 and Glu290, to the positively charged lysine in the K211E mutant. If activity is restored, this would imply that the structure of the K211E mutant is now reestablished and further prove that this residue is not directly involved in PGG_2 binding.

Single mutation of Lys215 and Lys222, either to alanine or glutamic acid, does not affect enzyme activity (Figure 7A). However, simultaneous mutation of these residues causes a significant decrease in activity. We propose that the presence of these two compensatory residues is a "safety mechanism" which highlights the importance of a positively charged region for substrate binding (*41*): if one of the lysines is mutated, the enzyme would still be fully functional as a substrate host due to the presence of the other lysine. Indeed, both residues are highly conserved in both isoforms of numerous species, and at least one of the two amino acids is always a lysine in mammals (Figure 5). Furthermore, this effect could not have been predicted from homology alignments as neither residue is entirely conserved. The average

40% decrease in activity of the double mutants with respect to the wild type correlates well with the ~2.0 kcal/mol decrease in binding energy due to the loss of the salt bridges predicted by docking calculations (Figure 7B).

It could be argued that the effect of simultaneous mutation of Lys215 and Lys222 may be due to nonspecific effects unrelated to ligand binding. Inspection of the crystal structure, however, indicates that Lys215 does not show significant interactions with any other residue of the protein, while Lys222 is only involved in hydrogen bonding with the poorly conserved Ser213 side chain. Furthermore, the fact that single mutations have no effect on enzyme activity indicates that these mutations do not have serious implications for enzyme folding.

The proposed binding model is, thus, fully consistent with the commonly accepted mechanism of catalysis as well as with our, and other previously reported, site-directed mutagenesis studies. On the basis of the binding model presented here, which defines the minimal pharmacophore for specific enzyme−substrate recognition, we have designed a first generation of PGHS−peroxidase inhibitors which are expected to be highly selective and become valuable chemical tools for exploring the implication of this peroxidase in pathophysiology. The synthesis and testing of these compounds are currently underway.

SUPPORTING INFORMATION AVAILABLE

GenBank accession numbers for proteins used in Figure 5 and the DNA sequencing data for the mutants. This material is available free of charge via the Internet at http://pubs.acs.org.

REFERENCES

1. Smith, W. L., Marnett, L. J., and DeWitt, D. L. (1991) Prostaglandin and thromboxane biosynthesis, *Pharmacol. Ther. 49*, 153−179.
2. Smith, W. L., DeWitt, D. L., and Garavito, R. M. (2000) Cyclooxygenases: structural, cellular, and molecular biology, *Annu. Rev. Biochem. 69*, 145−182.
3. Simmons, D. L., Botting, R. M., and Hla, T. (2004) Cyclooxygenase isozymes: the biology of prostaglandin synthesis and inhibition, *Pharmacol. Rev. 56*, 387−437.
4. Zhang, Y., Shaffer, A., Portanova, J., Seibert, K., and Isakson, P. C. (1997) Inhibition of cyclooxygenase-2 rapidly reverses inflammatory hyperalgesia and prostaglandin E2 production, *J. Pharmacol. Exp. Ther. 283*, 1069−1075.
5. Kargman, S. L., O'Neill, G. P., Vickers, P. J., Evans, J. F., Mancini, J. A., and Jothy, S. (1995) Expression of prostaglandin G/H synthase-1 and -2 protein in human colon cancer, *Cancer Res. 55*, 2556−2559.
6. Hida, T., Yatabe, Y., Achiwa, H., Muramatsu, H., Kozaki, K., Nakamura, S., Ogawa, M., Mitsudomi, T., Sugiura, T., and Takahashi, T. (1998) Increased expression of cyclooxygenase 2 occurs frequently in human lung cancers, specifically in adenocarcinomas, *Cancer Res. 58*, 3761−3764.
7. Parrett, M. L., Abou-Issa, H. M., Alshafie, G., Ross, M. S., Harris, R. E., and Robertson, F. M. (1999) Comparative ability of ibuprofen and N-(4-hydroxyphenyl)retinamide to inhibit development of rat mammary adenocarcinomas associated with differential inhibition of gene expression of cyclooxygenase isoforms, *Anticancer Res. 19*, 5079−5085.
8. Rich, J. B., Rasmusson, D. X., Folstein, M. F., Carson, K. A., Kawas, C., and Brandt, J. (1995) Nonsteroidal anti-inflammatory drugs in Alzheimer's disease, *Neurology 45*, 51−55.
9. Teismann, P., Tieu, K., Choi, D. K., Wu, D. C., Naini, A., Hunot, S., Vila, M., Jackson-Lewis, V., and Przedborski, S. (2003) Cyclooxygenase-2 is instrumental in Parkinson's disease neurodegeneration, *Proc. Natl. Acad. Sci. U.S.A. 100*, 5473−5478.
10. Linton, M. F., and Fazio, S. (2004) Cyclooxygenase-2 and inflammation in atherosclerosis, *Curr. Opin. Pharmacol. 4*, 116−123.
11. Tanabe, T., and Tohnai, N. (2002) Cyclooxygenase isozymes and their gene structures and expression, *Prostaglandins Other Lipid Mediators 68−69*, 95−114.
12. Funk, C. D., Funk, L. B., Kennedy, M. E., Pong, A. S., and Fitzgerald, G. A. (1991) Human platelet/erythroleukemia cell prostaglandin G/H synthase: cDNA cloning, expression, and gene chromosomal assignment, *FASEB J. 5*, 2304−2312.
13. Hla, T., and Neilson, K. (1992) Human cyclooxygenase-2 cDNA, *Proc. Natl. Acad. Sci. U.S.A. 89*, 7384−7388.
14. Chandrasekharan, N. V., Dai, H., Roos, K. L., Evanson, N. K., Tomsik, J., Elton, T. S., and Simmons, D. L. (2002) COX-3, a cyclooxygenase-1 variant inhibited by acetaminophen and other analgesic/antipyretic drugs: cloning, structure, and expression, *Proc. Natl. Acad. Sci. U.S.A. 99*, 13926−13931.
15. Garavito, R. M., Malkowski, M. G., and DeWitt, D. L. (2002) The structures of prostaglandin endoperoxide H synthases-1 and -2, *Prostaglandins Other Lipid Mediators 68−69*, 129−152.
16. Picot, D., Loll, P. J., and Garavito, R. M. (1994) The X-ray crystal structure of the membrane protein prostaglandin H2 synthase-1, *Nature 367*, 243−249.
17. Kulmacz, R. J., van der Donk, W. A., and Tsai, A. L. (2003) Comparison of the properties of prostaglandin H synthase-1 and -2, *Prog. Lipid Res. 42*, 377−404.
18. Kiefer, J. R., Pawlitz, J. L., Moreland, K. T., Stegeman, R. A., Hood, W. F., Gierse, J. K., Stevens, A. M., Goodwin, D. C., Rowlinson, S. W., Marnett, L. J., Stallings, W. C., and Kurumbail, R. G. (2000) Structural insights into the stereochemistry of the cyclooxygenase reaction, *Nature 405*, 97−101.
19. Thuresson, E. D., Lakkides, K. M., Rieke, C. J., Sun, Y., Wingerd, B. A., Micielli, R., Mulichak, A. M., Malkowski, M. G., Garavito, R. M., and Smith, W. L. (2001) Prostaglandin endoperoxide H synthase-1: the functions of cyclooxygenase active site residues in the binding, positioning, and oxygenation of arachidonic acid, *J. Biol. Chem. 276*, 10347−10357.
20. FitzGerald, G. A. (2003) COX-2 and beyond: Approaches to prostaglandin inhibition in human disease, *Nat. Rev. Drug Discov. 2*, 879−890.
21. Ullrich, V., and Ruf, H. H. (1994) Heme Proteins in Prostaglandin Biosynthesis, in *Metalloporphyrins in Catalytic Oxidations* (Sheldon, R. A., Ed.) pp 157−192, Marcel Dekker, New York.
22. O'Brien, P. J. (2000) Peroxidases, *Chem.-Biol. Interact. 129*, 113−139.
23. Lassmann, G., Odenwaller, R., Curtis, J. F., DeGray, J. A., Mason, R. P., Marnett, L. J., and Eling, T. E. (1991) Electron spin resonance investigation of tyrosyl radicals of prostaglandin H synthase. Relation to enzyme catalysis, *J. Biol. Chem. 266*, 20045−20055.
24. Tsai, A., Hsi, L. C., Kulmacz, R. J., Palmer, G., and Smith, W. L. (1994) Characterization of the tyrosyl radicals in ovine prostaglandin H synthase-1 by isotope replacement and site-directed mutagenesis, *J. Biol. Chem. 269*, 5085−5091.
25. Landino, L. M., Crews, B. C., Gierse, J. K., Hauser, S. D., and Marnett, L. J. (1997) Mutational analysis of the role of the distal histidine and glutamine residues of prostaglandin-endoperoxide synthase-2 in peroxidase catalysis, hydroperoxide reduction, and cyclooxygenase activation, *J. Biol. Chem. 272*, 21565−21574.
26. Markey, C. M., Alward, A., Weller, P. E., and Marnett, L. J. (1987) Quantitative studies of hydroperoxide reduction by prostaglandin H synthase. Reducing substrate specificity and the relationship of peroxidase to cyclooxygenase activities, *J. Biol. Chem. 262*, 6266−6279.
27. Wu, G., Wei, C., Kulmacz, R. J., Osawa, Y., and Tsai, A. L. (1999) A mechanistic study of self-inactivation of the peroxidase activity in prostaglandin H synthase-1, *J. Biol. Chem. 274*, 9231−9237.
28. Song, I., Ball, T. M., and Smith, W. L. (2001) Different suicide inactivation processes for the peroxidase and cyclooxygenase activities of prostaglandin endoperoxide H synthase-1, *Biochem. Biophys. Res. Commun. 289*, 869−875.
29. van der Donk, W. A., Tsai, A. L., and Kulmacz, R. J. (2002) The cyclooxygenase reaction mechanism, *Biochemistry 41*, 15451−15458.
30. Schneider, C., Boeglin, W. E., and Brash, A. R. (2004) Identification of two cyclooxygenase active site residues, Leucine 384 and Glycine 526, that control carbon ring cyclization in prostaglandin biosynthesis, *J. Biol. Chem. 279*, 4404−4414.

31. Malkowski, M. G., Ginell, S. L., Smith, W. L., and Garavito, R. M. (2000) The productive conformation of arachidonic acid bound to prostaglandin synthase, *Science 289*, 1933−1937.
32. Kukreja, R. C., Kontos, H. A., Hess, M. L., and Ellis, E. F. (1986) PGH synthase and lipoxygenase generate superoxide in the presence of NADH or NADPH, *Circ. Res. 59*, 612−619.
33. Reese, J., Paria, B. C., Brown, N., Zhao, X., Morrow, J. D., and Dey, S. K. (2000) Coordinated regulation of fetal and maternal prostaglandins directs successful birth and postnatal adaptation in the mouse, *Proc. Natl. Acad. Sci. U.S.A. 97*, 9759−9764.
34. Szewczuk, L. M., Forti, L., Stivala, L. A., and Penning, T. M. (2004) Resveratrol is a peroxidase-mediated inactivator of COX-1 but not COX-2: a mechanistic approach to the design of COX-1 selective agents, *J. Biol. Chem. 279*, 22727−22737.
35. Tam, S. S., Lee, D. H., Wang, E. Y., Munroe, D. G., and Lau, C. Y. (1995) Tepoxalin, a novel dual inhibitor of the prostaglandin-H synthase cyclooxygenase and peroxidase activities, *J. Biol. Chem. 270*, 13948−13955.
36. Seibold, S. A., Smith, W. L., and Cukier, C. I. (2004) The peroxidase site of prostaglandin endoperoxide H synthase-1 docking and molecular dynamic studies with a prostaglandin endoperoxide analog, *J. Phys. Chem. B. 108*, 9297−9305.
37. Gupta, K., Selinsky, B. S., Kaub, C. J., Katz, A. K., and Loll, P. J. (2004) The 2.0 Å resolution crystal structure of prostaglandin H2 synthase-1: structural insights into an unusual peroxidase, *J. Mol. Biol. 335*, 503−518.
38. Morris, G. M., Goodsell, D. S., Halliday, R. S., Huey, R., Hart, W. E., Belew, R. K., and Olson, A. J. (1998) Automated docking using a Lamarckian genetic algorithm and empirical binding free energy function, *J. Comput. Chem. 19*, 1639−1662.
39. Schwede, T., Kopp, J., Guex, N., and Peitsch, M. C. (2003) Swiss-Model: An automated protein homology-modeling server, *Nucleic Acids Res. 31*, 3381−3385.
40. Jones, P. (2001) Roles of water in heme peroxidase and catalase mechanisms, *J. Biol. Chem. 276*, 13791−13796.
41. Riordan, J. F., McElvany, K. D., and Borders, C. L. (1977) Arginyl residues: anion recognition sites in enzymes, *Science 195*, 884−886.
42. Rudberg, P. C., Tholander, F., Andberg, M., Thunnissen, M. M., and Haeggstrom, J. Z. (2004) Leukotriene A4 hydrolase: identification of a common carboxylate recognition site for the epoxide hydrolase and aminopeptidase substrates, *J. Biol. Chem. 279*, 27376−27382.
43. Smith, T., Leipprandt, J., and DeWitt, D. (2000) Purification and characterization of the human recombinant histidine-tagged prostaglandin endoperoxide H synthases-1 and -2, *Arch. Biochem. Biophys. 375*, 195−200.
44. Roth, G. J., Machuga, E. T., and Ozols, J. (1983) Isolation and covalent structure of the aspirin-modified, active-site region of prostaglandin synthetase, *Biochemistry 22*, 4672−4675.
45. Thompson, J. D., Higgins, D. G., and Gibson, T. J. (1994) ClustalW: improving the sensitivity of progressive multiple sequence alignment through sequence weighting, position-specific gap penalties and weight matrix choice, *Nucleic Acids Res. 22*, 4673−4680.
46. Dooley, C. M., Devocelle, M., McLoughlin, B., Nolan, K. B., Fitzgerald, D. J., and Sharkey, C. T. (2003) A novel family of hydroxamate-based acylating inhibitors of cyclooxygenase, *Mol. Pharmacol. 63*, 450−455.
47. Chubb, A. J., Schwager, S. L., van der Merwe, E., Ehlers, M. R., and Sturrock, E. D. (2004) Deletion of the cytoplasmic domain increases basal shedding of angiotensin-converting enzyme, *Biochem. Biophys. Res. Commun. 314*, 971−975.
48. Pettersen, E. F., Goddard, T. D., Huang, C. C., Couch, G. S., Greenblatt, D. M., Meng, E. C., and Ferrin, T. E. (2004) UCSF Chimera—a visualization system for exploratory research and analysis, *J. Comput. Chem. 25*, 1605−1612.
49. Sanner, M. F., Olson, A. J., and Spehner, J. C. (1996) Reduced surface: an efficient way to compute molecular surfaces, *Biopolymers 38*, 305−320.

BI051973K